AD-A071 354 DEFENCE RESEARCH ESTABLISHMENT PACIFIC VICTORIA (BRIT--ETC F/G 20/1
ACOUSTIC PHASE FLUCTUATIONS CAUSED BY GARRETT-MUNK INTERNAL WAV--ETC(U)
MAR 79 B HUGHES

UNCLASSIFIED DREP-TM-79-1 NL

| OF |
AD
A071354

END
DATE
FILMED
8 --79
DDC

Victoria, B.C.

LEVEL II

Technical Memorandum 79-1

ACOUSTIC PHASE FLUCTUATIONS CAUSED BY GARRETT–MUNK INTERNAL WAVES

B. Hughes

March 1979

Research and Development Branch
Department of National Defence
Canada

DEFENCE RESEARCH ESTABLISHMENT PACIFIC

VICTORIA, B.C.

DREP Technical Memorandum 79-1

(9) Technical memo.

(6) ACOUSTIC PHASE FLUCTUATIONS CAUSED BY GARRETT-MUNK INTERNAL WAVES.

(10) B. Hughes

(12) 35 p.

(11) March 1979

(14) DREP-TM-79-1

Approved by:

R.A. Kendall

RESEARCH AND DEVELOPMENT BRANCH
DEPARTMENT OF NATIONAL DEFENCE
CANADA

403 246

JCB

ABSTRACT

Perturbed acoustic propagation is considered between a point source and an array receiver in which the perturbations are due to a Garrett-Munk internal wave field. The resultant acoustic phase fluctuations along the array are determined. Straight ray propagation is assumed, and three array orientations are considered: broadside horizontal, endfire horizontal and broadside vertical. It is shown that for an acoustic frequency of 150 Hz, a range of 50 km and a horizontal broadside receiver separation distance (in the array) of 1 km, the rms phase difference between the two receivers at 1000 m depth in the N. Pacific is typically 5°, and in the Arctic it is typically 2°, whereas in the N. Atlantic at the same depth it is typically 50°. These geographical variations are due mainly to variations in the potential sound velocity gradient. Similar phase differences occur for a vertical receiver separation of 50 m. The horizontal receiver separation necessary to reduce the acoustic coherence to 0.5 for the same operating conditions is shown to be very large in the N. Pacific (≅ 400 km) and Arctic (> 1000 km), but only 2.3 km in the N. Atlantic.

INTRODUCTION

Any system which makes use of phase comparisons in underwater acoustic signals will ultimately be limited in its accuracy by the randomizing effect of the natural state of motion in the ocean medium. In recent years, this state of motion has been the subject of much research, particularly for those length and time scales than can be described as internal waves. One of the results of this research is that there now exists an analytic model than can be used to predict acoustic properties of the ocean, such as the expected rms acoustic fluctuations, the coherence lengths, frequency and wavenumber spectra, etc. The internal wave model, known as the Garrett-Munk spectrum (Desaubies, 1976a and b), is empirically based and has been subjected to some experimental confirmation since its proposal (for a general reference see the collection of papers edited by Briscoe (1975)).

If an acoustic signal is transmitted over a fixed path between two points, the phase difference between the received and transmitted signals will be dependent on a number of variables, for example: signal frequency, path length, the total sound velocity structure, receiver and source depth, etc. If the sound velocity structure is unvarying in time, a signal at a given frequency will exhibit an unvarying phase difference. If the sound velocity structure changes in time, the given signal will exhibit varying phase differences, and the characteristics of the variation will be intimately linked to the characteristics of the velocity changes. If the sound velocity changes are due to background internal waves, they will be distributed along the entire acoustic path and the resultant phase difference at the receiver will be an integral of these changes taken along the path. In the treatment given here the acoustic

phase perturbation is defined as the extra amount of phase difference caused solely by the presence of the internal waves.

The internal wave field is modelled stochastically, that is, only expected values are known, and the internal wave field at any given instant is merely one unspecified realization taken from an infinite ensemble of such realizations. The acoustic phase perturbation is thus a random process and, therefore, only expected values can be predicted.

Two papers have recently been published that deal extensively with this acoustic perturbation problem. They provide overlapping treatments and so they will be discussed here together. The first is by Munk and Zachariasen (1976), hereafter referred to as MZ, the second is by Desaubies (1976a). In these papers, the authors have shown that for the two-point fixed-geometry single-receiver acoustic transmission situation referred to above, the expected rms phase perturbation caused by internal waves is proportional to the signal frequency and approximately proportional to the square root of the path length. The proportionality constants are governed by parameters from the internal wave model. They have also shown that the perturbations change very slowly in time; the frequency spectrum of the phase perturbations is heavily weighted towards the inertial period (15.7 hrs at 50°N and 12 hrs at 90°N).

For this single-receiver configuration then, and assuming no other perturbations are present, the received phase will appear to be stable over short time periods (say ½ hr or less), although the value of the received phase will be different from the unperturbed value by a random amount with a root-mean-square that is governed by the internal wave field parameters and details of the configuration.

For an array receiver configuration and a single source, Figure 1, the received phase at any single hydrophone will also appear to be stable

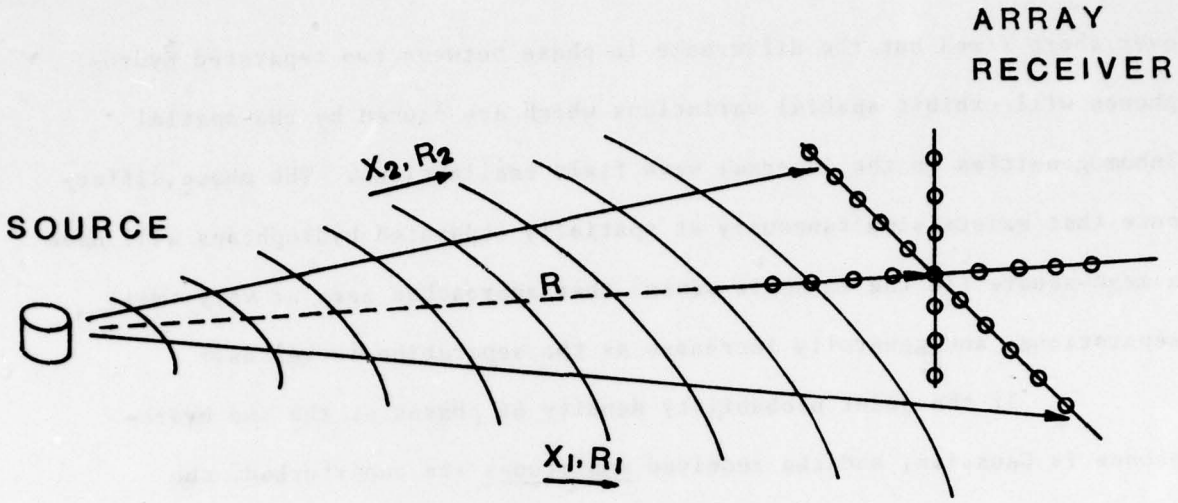

INTERNAL WAVES ABSENT

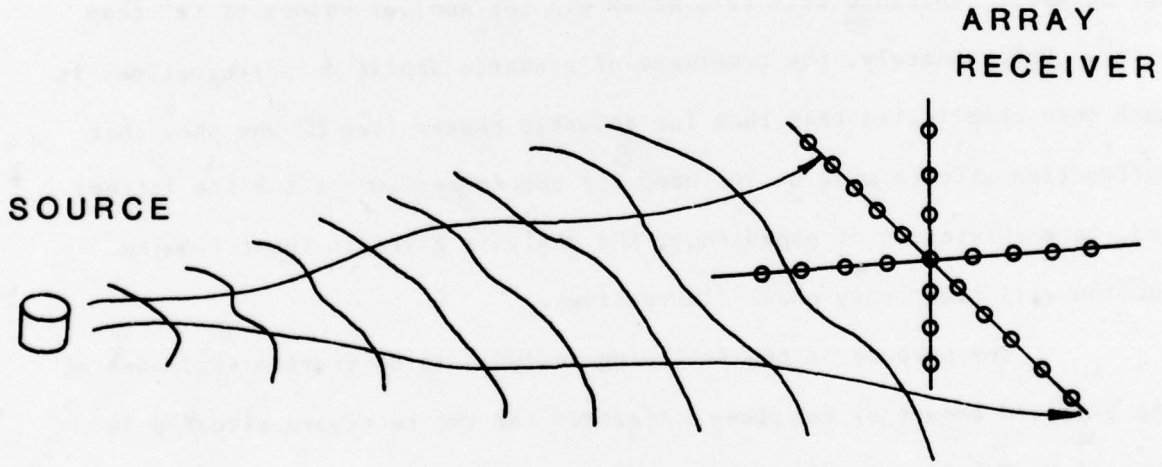

INTERNAL WAVES PRESENT

Figure 1. Schematic representation of the propagation configuration.

over short times but the difference in phase between two separated hydrophones will exhibit spatial variations which are caused by the spatial inhomogeneities in the internal wave field realizations. The phase difference that exists simultaneously at spatially separated hydrophones will have a mean-square (in the ensemble sense) that approaches zero at very small separations, and generally increases as the separation increases.

If the joint probability density of phases at the two hydrophones is Gaussian, and the received amplitudes are unperturbed, the coherence between the two received acoustic signals will be $\exp\{-\frac{1}{2}\phi^2\}$, where ϕ^2 is the mean-square phase difference. Thus, the acoustic coherence will be less than 0.5 whenever the rms phase difference is larger than 67.4°. Of course, in a real propagation situation, the acoustic amplitudes are also expected to be randomized by the internal wave field with the result that the acoustic coherence will fall below 0.5 for smaller values of $\sqrt{\phi^2}$ than 67.4°. Unfortunately, the treatment of acoustic amplitude perturbations is much more complicated than that for acoustic phases (see MZ who show that diffraction effects must be included for the former but not for the latter) and, in the interest of expediency, the analysis given in the following section will treat only phase fluctuations.

The purpose of the following analysis is to provide estimates of the expected amount of rms phase difference for two receivers situated in typical N. Pacific, Arctic and N. Atlantic conditions. Three array orientations will be considered: endfire horizontal, broadside horizontal, and broadside vertical. The numerical estimates are obtained by using straight ray approximations and the Garrett-Munk spectrum.

The receiver separation necessary to reduce the acoustic coherence to 0.5 (i.e. rms phase difference = 67.4°) is calculated for the above

conditions for a horizontal broadside array at a range of 50 km; and predictions are also made (in Appendix A) using a variant of the Garrett-Munk spectrum due to Desaubies.

Surface and bottom reflections are specifically excluded from all calculations.

FLUCTUATION MECHANISM

There are two predominant mechanisms by which internal waves can affect acoustic signals: (i) raising and lowering of surfaces of constant sound velocity, and (ii) Doppler shifts and advection due to fluid particle flow. It is shown by MZ that the former is an order of magnitude more important than the latter so only the former will be treated here. The wave equation for sound propagation in the absence of advection is

$$\frac{\partial^2 p}{\partial t^2} - c^2 \nabla^2 p = 0, \tag{1}$$

and in the presence of internal waves (or any perturbing agency)

$$c^2 = \Big(c_o(z) + \delta c(x,y,z,t) \Big) \approx c_o^2(z) + 2c_o(z)\, \delta c$$

$$= c_o^2(z) \{1 + 2\delta c/c_o\} \tag{2}$$

In these equations p is acoustic pressure, c is sound speed and c_o is unperturbed sound speed.

It is shown by MZ and Desaubies (1976a) that the effect of the inhomogeneities, δc, on the phase of p can be calculated by ray tracing or ray timing techniques (at least for paraxial rays).

From the ray model, the travel time T from source to a single receiver is given by

$$T = \int_o^R \frac{dr}{c} \approx \frac{1}{c_o} \int_o^R \frac{c_o - \delta c}{c_o} \, dr,$$

or

$$\delta T = -\frac{1}{c_o} \int_o^R \frac{\delta c}{c_o} \, dr. \tag{3}$$

In expressions (2) and (3), the δ-operator refers to differences between different realizations of the acoustic medium, and the integrals are taken along the mean ray path. The phase $\underline{\Phi}$ associated with δT is $\omega \delta T$ where ω is the radian acoustic frequency, therefore

$$\underline{\Phi} = -\frac{\omega}{c_o} \int_o^R \left(\frac{\delta c}{c_o}\right) dr. \tag{4}$$

The sound velocity perturbations are caused by vertical shifting of isovelocity contours, therefore it is expected that δc will simply be proportional to the product of the internal wave amplitude ζ and the background sound velocity gradient; that is

$$\frac{\delta c}{c_o} \approx \frac{\zeta}{c_o} \frac{\partial c_o}{\partial z} \tag{5}$$

Although this relation is conceptually correct, it is shown by Munk (1974) that the gradient $\partial c_o / \partial z$ should actually be replaced by the gradient of <u>potential</u> sound velocity $\partial c_p / \partial z$ where c_p does not include pressure effects or the effect of the adiabatic lapse rate.

The corrected version of (5) can be substituted in (4) giving

$$\underline{\Phi}(R) = -\frac{\omega}{c_o}\int_o^R \left(\frac{\partial c_p}{c_o \partial z}\right) \zeta(\vec{x}(r))\, dr \qquad (6)$$

The mean-square phase difference between two spatially separated receivers is given by

$$\phi^2 = \langle [\underline{\Phi}(R_2) - \underline{\Phi}(R_1)]^2 \rangle,$$

which, by (6), becomes

$$\begin{aligned}\phi^2 = \frac{\omega^2}{c_o^2}\Bigg[&\int_o^{R_1}\int_o^{R_1} \left\{ \frac{\partial c_p(\vec{x}_1)}{c_o \partial z} \quad \frac{\partial c_p(\vec{x}_2)}{c_o \partial z} \right\} \langle \zeta(\vec{x}_1)\zeta(\vec{x}_2) \rangle \, dr_1 dr_2 \\ &+ \int_o^{R_2}\int_o^{R_2} \left\{ \frac{\partial c_p(\vec{x}_1)}{c_o \partial z} \quad \frac{\partial c_p(\vec{x}_2)}{c_o \partial z} \right\} \langle \zeta(\vec{x}_1)\zeta(\vec{x}_2) \rangle \, dr_1 dr_2 \qquad (7) \\ &- 2\int_o^{R_1}\int_o^{R_2} \left\{ \frac{\partial c_p(\vec{x}_1)}{c_o \partial z} \quad \frac{\partial c_p(\vec{x}_2)}{c_o \partial z} \right\} \langle \zeta(\vec{x}_1)\zeta(\vec{x}_2) \rangle \, dr_1 dr_2 \end{aligned}$$

In order to determine typical values of ϕ^2, several assumptions will now be invoked, namely, straight acoustic rays, constant $\partial c_p / c_o \partial z$, and stationary $\langle \zeta(\vec{x}_1)\zeta(\vec{x}_2) \rangle$ given in terms of the Garrett-Munk spectrum. The assumption of straight acoustic rays can be relaxed somewhat. Desaubies (1976b) shows that ray curvature per se is mostly unimportant in treating phase perturbation; however, the assumption of constant $\partial c_p / c_o \partial z$ and uniform $\langle \zeta^2 \rangle$ (in depth) are important and are not trivially removed. Further comments are given in the discussion.

The derivation of the final expression for ϕ^2 is given in Appendix B; the result is

$$\phi^2 = \left\{4\pi \frac{\lambda(90^o)}{\lambda_{acoustic}} \frac{\partial c_p}{c_o \partial z} \zeta_{rms}\right\}^2 T \tag{8a}$$

$$\phi^2 = \left(\frac{\omega}{c_o}\right)^2 \left(\frac{\partial c_p}{c_o \partial z}\right)^2 \frac{2}{\pi} E\, b^2 \left(\frac{n_o}{n}\right) \lambda^2(90^o) \left\{\tan^{-1}\sqrt{\mu^2 - 1} - \sqrt{\frac{\mu^2 - 1}{\mu^2}}\right\}$$
$$T\left(\frac{\Delta}{\lambda(\theta_2)}, \frac{R}{\lambda(90^o)}, \mu, \theta_1, \theta_2\right) \tag{8b}$$

where the terms E and b come from the internal wave spectrum, R is the median source-receiver range, n_o is the Brunt-Väisälä frequency just below the thermocline, n is the Brunt-Väisälä frequency at the transmission depth, μ is n/n_{in}, n_{in} is the local inertial frequency, Δ is the receiver separation distance, θ_1 is the angle between the array axis and the median propagation direction, θ_2 is the angle between the array axis and vertical, and $\lambda(\theta_2)$ is the relevant internal wave length scale, which, because of vertical anisotropy in the Garrett-Munk spectrum, is dependent on the angle θ_2. The function T contains the entire dependence of ϕ^2 on receiver separation, Δ, receiver orientation, and source-receiver range, R. This dependence is illustrated in Figure 2 for a horizontal array in endfire orientation ($\theta_1=0^o$, $\theta_2=90^o$), in Figure 3 for a horizontal array in broadside orientation ($\theta_1=90^o$, $\theta_2=90^o$), and in Figure 4 for a vertical array in broadside orientation ($\theta_1=90^o$, $\theta_2=90^o$). In Figure 2 there is no range dependence; each curve refers to a different value of $\mu(=n(z)/n_{in})$ as indicated. In Figures 3 and 4, λ_H is $\lambda(90^o)$, λ_v is $\lambda(0^o)$, each group of curves pertains to a different range ($\log R/\lambda_H$ is given for each group), and within each group, each curve pertains to a different μ (as shown on right side). For

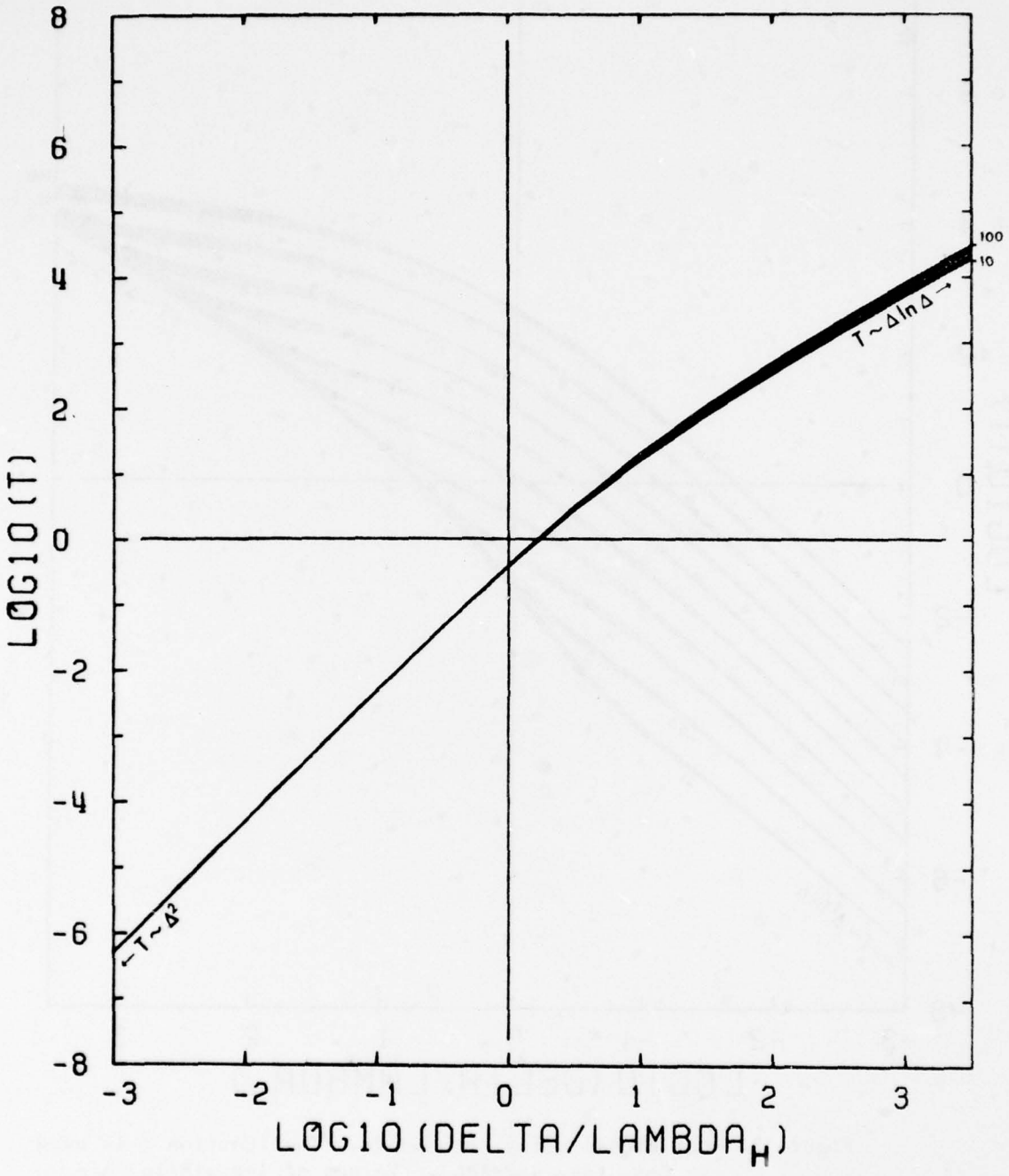

Figure 2. Horizontal array, endfire. The function T is used in Eqs. (8a) and (8b). Seven curves are shown; each pertains to a different value of μ, and the smallest and largest μ-values used are indicated on the right.

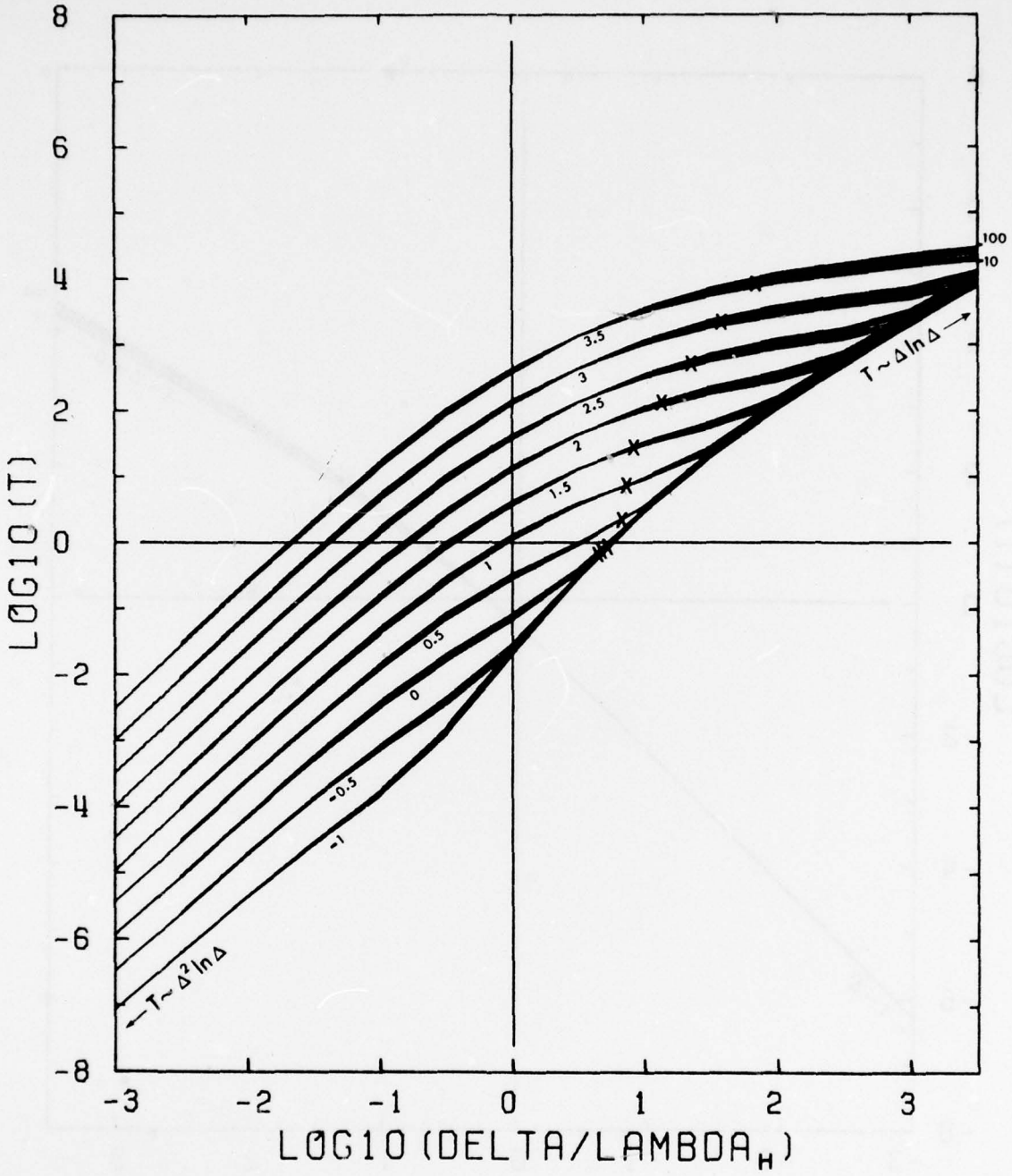

Figure 3. Horizontal array, broadside. The function T is used in Eqs. (8a) and (8b). Values of $\log_{10}(R/\lambda_H)$ are given for each group of curves. Within each group, seven curves are shown, each for a different value of μ, and the smallest and largest μ-values used are indicated on the right for one of the groups. The crosses indicate separations at which the acoustic phase correlation is 0.5 (not to be confused with acoustic signal correlation).

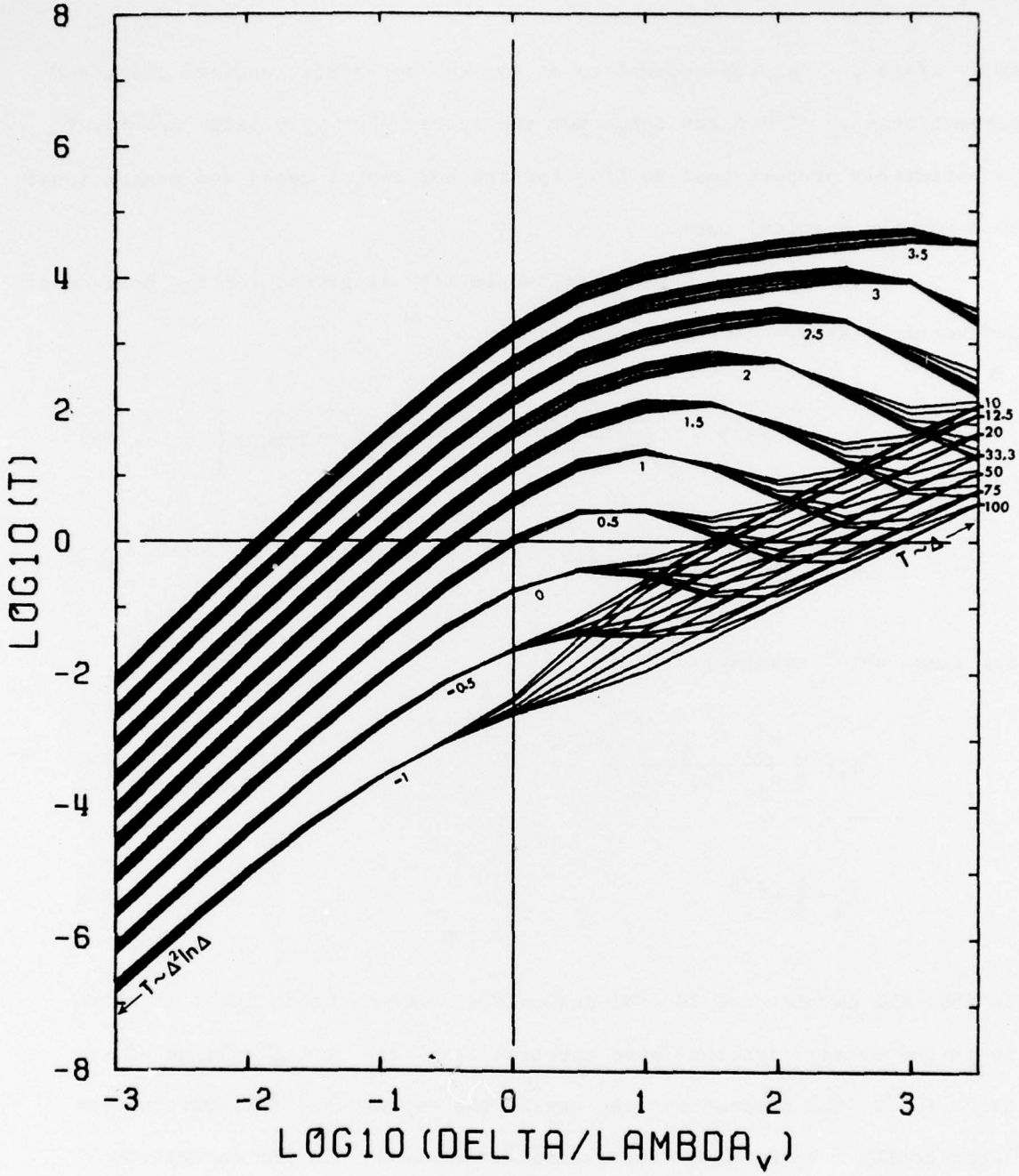

Figure 4. Vertical array, broadside. The function T is used in Eqs. (8a) and (8b). Values of $\log_{10}(R/\lambda_H)$ are given for each group of curves. Values of μ are given on the right for each curve.

small $\Delta/\lambda(\theta)$, T is proportional to Δ^2 for the horizontal endfire case, and porportional to $\Delta^2 \ln \Delta$ for the other two cases. For very large $\Delta/\lambda(\theta)$, T is ultimately proportional to $\Delta \ln \Delta$ for the horizontal cases and proportional to Δ for the vertical case.

The internal wave length scale $\lambda(\theta)$ is given, for the horizontal and vertical array cases respectively, by

$$\lambda_H = \lambda(90^o) = b \frac{n_o}{12 n_{in}} \left\{ \frac{\tan^{-1}\sqrt{\mu^2 - 1} - \sqrt{\mu^2 - 1}/\mu^2}{\ln \mu - (\mu^2 - 1)/2\mu^2} \right\} , \qquad (9a)$$

$$\lambda_V = \lambda(0^o) = b \frac{1}{3\pi} e^{z/b} , \qquad (9b)$$

or, since $\mu >> 1$ usually,

$$\lambda_H \sim \frac{b}{8} \frac{n_o}{n_{in}} \frac{1}{\ln\mu - \frac{1}{2}} , \qquad (9c)$$

$$\lambda_V \sim \frac{b}{9} e^{z/b} . \qquad (9d)$$

In (8b) the parameter E is a dimensionless "universal constant"; it represents the overall internal wave spectral level and it has a value of 5.3×10^{-5}. The parameter b represents the exponential fall-off rate at large depths for the mean Brunt-Väisälä frequency. In the Garrett-Munk internal wave spectral model, the Brunt-Väisälä frequency n(z) is taken to be

$$n(z) = n_o e^{-z/b} \qquad (10)$$

in the main body of the ocean (i.e. below the thermocline).

It can be seen from Figures 2 to 4 that the rate of increase of T with Δ begins to reduce near $\Delta \approx \lambda(\theta)$ (for fixed R/λ_H). This occurs because the correlation between the phase parts of the signals at the two receivers, which is almost unity for $\Delta < \lambda(\theta)$, begins a more rapid decrease as Δ increases, and, as Δ becomes larger than $\lambda(\theta)$, the correlation becomes significantly less than unity. The phase correlation distance, that is, the value of Δ at which the correlation of the phases is 0.5, is not reached, however, until $\Delta/\lambda(\theta)$ has increased to the value indicated by the cross (for each R/λ_H curve).

For the vertical array configuration, T actually decreases as Δ increases, for $\Delta/\lambda_v \gtrsim 1$. More specifically, this behaviour exists for a particular range of ray angles, measured with respect to the horizontal, namely $10^o \lesssim |\text{ray angle}| \lesssim 85^o$, or $1 < (\Delta/R)(\lambda_H/\lambda_v) \lesssim 100$. The reduction occurs because λ_H is significantly greater than λ_v. For almost horizontal propagation, the phase coherence length is controlled by the horizontal internal wave coherence length λ_H. As Δ increases with R fixed, the effective coherence length tends towards λ_v, i.e., it reduces significantly, with the result that significantly more of the phase fluctuation cancels itself out when integrated along the total ray path. For $\Delta >> \lambda(\theta)$, T again increases, but this is because in this regime the actual propagation range $\sqrt{R^2 + \frac{1}{4}\Delta^2}$, significantly increases with Δ, along each constant R/λ_H curve, and it more than compensates for any reduction tendencies.

The parameter $\lambda(\theta)$ thus serves to divide the separation distances into two regions: one region includes the very tightly correlated separations where T is small but increases rapidly; the other includes the more loosely correlated separation where T is more nearly its maximum and increases much more slowly (not including very large Δ).

The range dependence of T can be summarized as follows: for the endfire case T is range independent; for the horizontal and vertical broadside cases, T is proportional to R ln R for R and $\Delta \to 0$, it is range independent for $\Delta/\lambda(\theta) \to \infty$, and it is proportional to R between these two limiting cases. For the endfire case the two rays are identical between the source and the nearest receiver and thus the phase difference generated over this part of the propagation path is zero. The entire phase difference is due only to propagation between the two receivers and hence is independent of the source-receiver distance. For the other two cases the range-independence at very large $\Delta/\lambda(\theta)$ occurs because $\Delta >> R$ is the regime and so the total propagation path length $\sqrt{R^2 + \frac{1}{4}\Delta^2}$ is virtually independent of R; in the more interesting regime of small $\Delta/\lambda(\theta)$, the R ln R or R-dependence is due to the detailed form of the Garrett-Munk internal wave spectrum.

For $\Delta/\lambda(\theta) \approx 1$, Figures 2 to 4 show that

$$\sqrt{T} \approx \begin{cases} 0.4\ \Delta/\lambda_H & \text{for endfire horizontal,} \\ 0.4\sqrt{\Delta R/\lambda_H} & \text{for broadside horizontal,} \\ 0.4\sqrt{\frac{\Delta}{\lambda_v}\frac{R}{\lambda_H}} & \text{for broadside vertical.} \end{cases} \tag{11}$$

By using (11) for this range of Δ, and by taking the square root of (8b), it can be seen that the rms phase difference, rms ϕ, is proportional to the potential sound velocity gradient $\partial c_p/\partial c$, the acoustic frequency $f_a (=\omega/2\pi)$, the square root of the oceanographic length scale b and either Δ or $\sqrt{\Delta R}$ depending on the configuration. It is also proportional to the factor $e^{z/2b}$ and a term dependent only on μ. This is summarized as follows: for $\Delta/\lambda(\theta) \approx 1$ and $f_a/c_o \equiv \lambda_a$, the acoustic wavelength,

$$\text{rms } \phi \approx$$

$$e^{x/2b}\left(\frac{b}{c_o}\frac{\partial c_p}{\partial z}\right)\sqrt{\frac{2}{\pi}\left\{\tan^{-1}\sqrt{\mu^2-1}-\sqrt{\mu^2-1}/\mu^2\right\}}\begin{cases}\frac{\Delta}{\lambda_a} & \text{endfire horizontal.}\\ \sqrt{\frac{\Delta R}{\lambda_a}} & \text{broadside horizontal.}\\ \sqrt{\frac{\lambda_H}{\lambda_v}}\sqrt{\frac{\Delta R}{\lambda_a}} & \text{broadside vertical.}\end{cases} \tag{12}$$

where rms ϕ is given in degrees. The product of the first three terms in (12) is $\zeta_{rms}\frac{\partial c_p}{c_o \partial z}\Big/\sqrt{E}$, where ζ_{rms} is the local rms internal wave height, and it has been shown elsewhere (e.g. see Desaubies, 1976b Eq. 11 or MZ Eq. 89) that although ζ_{rms} is expected to increase with depth as $e^{z/2b}$, $\frac{\partial c_p}{c_o \partial z}$ is expected to decrease with depth as $e^{-2z/b}$ (at least for the profile given in 10). This leads to the conclusion that rms ϕ is expected to decrease with depth approximately as $e^{-1.5z/b}$. Thus, for straight ray propagation, more scattering by internal waves should occur for shallow paths than deep paths.

Curved rays are treated for a single receiver by MZ who give an exhaustive treatment of scattering in convergence zone propagation (excluding reflections). They find that most of the scattering occurs near the apex of the ray paths. The reason again is that $\zeta \partial c_p/\partial z$ follows a similar exponential depth-dependence as the Brunt-Väisälä frequency (Eq. 10) and so the internal waves produce more scattering (possibly orders of magnitude more) near the thermocline than in abyssal regions.

Desaubies (1976a) has provided an interesting and very attractive variant of the Garrett-Munk spectrum. He shows that the three parameters E, N_o and b can be reduced to two parameters r and t (using his notation) with

$$r = E\, n_o\, b^2 \tag{13}$$

$$t = 3/(2bn_o) \quad . \qquad (14)$$

With these definitions, the dependence of n^2 on z need not be exponential but may remain unspecified and completely general. The scaling parameters in the spectrum cease to be E, n_o, n_{in} and b and become r, t (neither of which is dimensionless), n_{in} and the local frequency n(z). He further shows that the existing data strongly suggest that r and t are universal constants with values of 300 m^2cph and 3.10^{-4} (cycles per meter) /cph respectively. This is equivalent to fixing the values of n_o and b, by equations (13) and (14) to be universally 4.42 cph and 1132 m respectively, and replacing $e^{z/b}$ by 4.42/n(z) where n(z) is left unspecified. In Appendix A, Equations (8b), (9) and (12) are rewritten using the r, t scaling.

TYPICAL OCEANIC PARAMETERS

Numerical estimates will now be obtained for four different oceanic regions, see Figure 5; the Gulf of Alaska (North Pacific), the Newfoundland Basin (North Central Atlantic), Robeson Channel in April (82°N, 60°W in the Eastern Arctic), and the Canada Basin in April (78°N, 130°W in the Western Arctic). In each region estimates are obtained for an acoustic frequency f_a of 150 Hz, a range R of 50 km and a hydrophone spacing of either 1 km for the horizontal separations or 50 m for the vertical separation.

Internal wave measurements in the temperate oceans indicate that $E = 5.3\ 10^{-5}$, and, in the absence of Arctic measurements, this value will be used for the Arctic case as well. Table I contains all the numerical values that have been used. The Gulf of Alaska and Newfoundland Basin data were calculated from temperature and salinity profiles published by Hashimoto (1968, his regions D and P respectively). At the chosen depth (1000 m) the

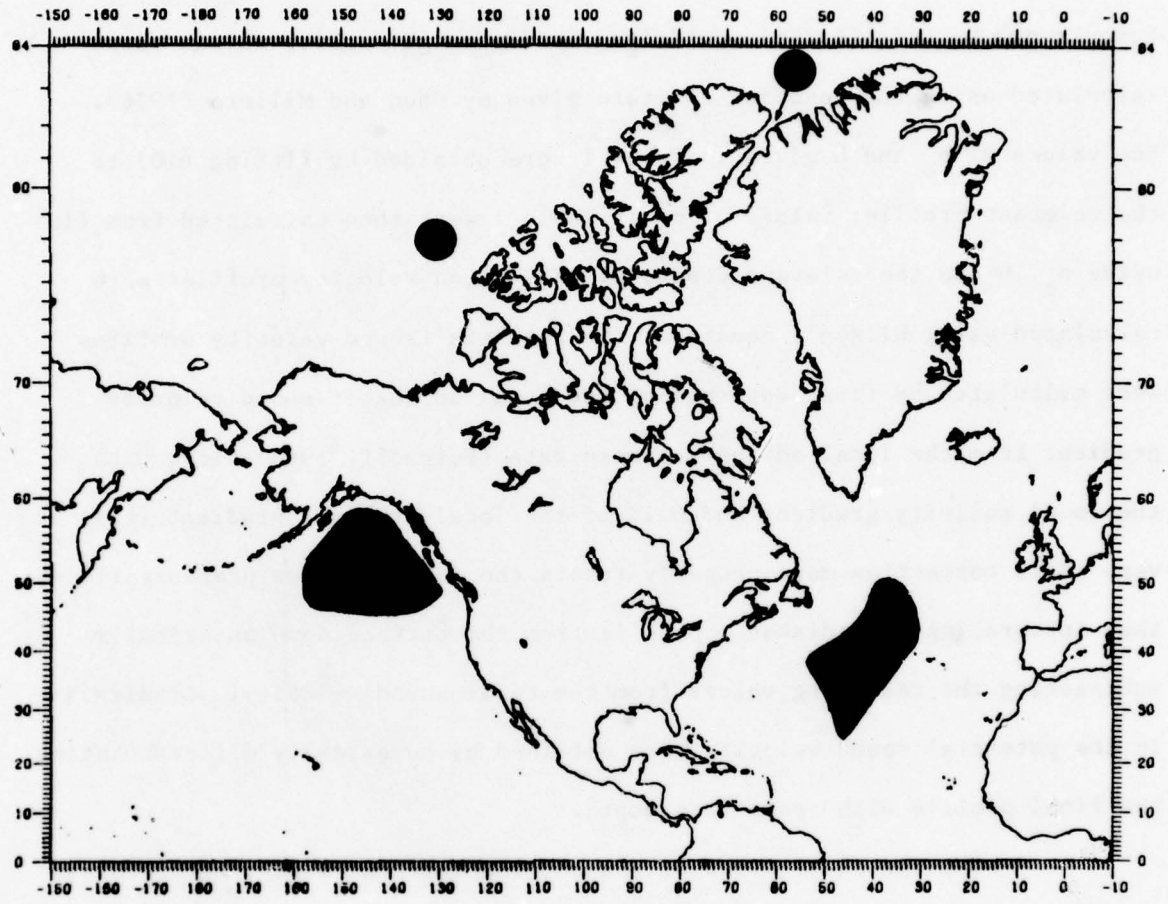

Figure 5. The solid regions indicate the locations of the four numerical examples: Gulf of Alaska (North Pacific), Newfoundland Basin (North Central Atlantic), Robeson Channel (82°N, 60°W), and Canada Basin (78°N, 130°W).

profiles are independent of season. The Robeson Channel data were calculated from temperature, salinity and density profiles published by Sadler (1976, his Figure 23) and the Canada Basin data were taken from Herlinveaux (1963, Station 1, Camp 1). All n(z) profiles were calculated using the formula $n^2(z) = (g/\zeta)(\partial\zeta/\partial z) - g^2/c^2(z)$, and <u>in situ</u> density values were calculated using the equation of state given by Chen and Millero (1976). The values of n_o and b given in Table I were obtained by fitting (10) to the relevant profile; values of n_o in Table I were then calculated from (10) using n_o, b and the relevant depth, z. The sound velocity profiles were calculated using Wilson's equation; the potential sound velocity profiles were calculated by first determining the local adiabatic sound velocity gradient from the local adiabatic lapse rate (Fofonoff, 1962) along with the local salinity gradient and 0.1% of the local pressure gradient (this very small correction more properly treats the internal wave pressure field), then integrating the adiabatic profile from the surface down and finally subtracting the resulting values from the total sound velocity. Gradients in the potential sound velocity were obtained by numerically differentiating the final profile with respect to depth.

The rms phase fluctuations and the internal wave length scales calculated* from these data are given in Table II. The most striking result is the comparatively large phase instability estimated for the Newfoundland Basin. It is a direct result of the relatively large potential sound gradient existing in that region which in turn may be due to its more southerly location. The other estimates are more uniform, with the Arctic

---

* Values equivalent to Table II, but using Desaubies' modified scaling are given in Appendix A.

TABLE I

OCEANOGRAPHIC DATA USED IN THE NUMERICAL EXAMPLES

Region and Depth	b(m)	$\frac{\partial c_p}{c_o \partial z}$ (m^{-1})	c_o(m/s)	n_o(cph)	n(cph)	n_{in}(cph)
Gulf of Alaska (1000 m)	1900	$-3.51\ 10^{-6}$	1477	2	1.18	$\frac{1}{15.7}$
Newfoundland Basin (1000 m)	2200	$-41.5\ 10^{-6}$	1501	3	1.90	$\frac{1}{17.0}$
Robeson Channel (April, 300 m)	86	$+3.95\ 10^{-6}$	1453	30	0.90	$\frac{1}{12.0}$
Canada Basin (April, 1000 m)	1000	$-1.53\ 10^{-6}$	1466	2	0.74	$\frac{1}{12.0}$

TABLE II

RESULTS FOR A RANGE OF 50 KM, AN ACOUSTIC FREQUENCY OF 150 HZ AND A RECEIVER SEPARATION OF EITHER 1 KM (HORIZONTAL CASES) OR 50M (VERTICAL CASE)

Region and Depth	Horizontal Broadside, rms $\phi = \langle [\Phi(R_2)-\Phi(R_1)]^2 \rangle^{\frac{1}{2}}$			λ_H	λ_V
	Endfire Horizontal	Broadside Horizontal	Broadside Vertical		
Gulf of Alaska (1000 m)	1.5°	4.6°	3.9°	3.0 km	340 m
Newfoundland Basin (1000 m)	20°	53°	65°	4.7 km	370 m
Robeson Channel (April 300 m)	0.31°	1.2°	0.71°	1.9 km	300 m
Canada Basin (April 1000 m)	0.40°	1.5°	0.86°	1.6 km	290 m

being more stable and having somewhat shorter internal wave length scales. The increased stability in the Arctic is due to weaker internal wave activity, as predicted by the Garrett-Munk model; the gradients of c_p are, in fact, almost the same as the Gulf of Alaska value.

Under the assumption that the internal wave statistics are Gaussian, the acoustic signal coherence between the two receivers drops to 0.5 when rms ϕ reaches 67.4° (keeping acoustic amplitudes fixed). Figure 6 illustrates the dependence of receiver separation on horizontal median-ray range for an acoustic signal coherence of 0.5 for each of the four oceanic regions. Only horizontal, broadside separation is shown, and, again the frequency is 150 Hz. In the N. Atlantic, short to moderate ranges produce a coherence of 0.5 (e.g. 50 km range, 2.3 km separation), in the N. Pacific the ranges and separation are considerably larger (e.g. 60 km range and 30 km separation), and in the Arctic the range and separation are so large that they are probably outside the framework of this analysis.

DISCUSSION AND CONCLUSIONS

Internal waves cause phase decorrelations between signals transmitted by a single source and received simultaneously by two separated hydrophones. The rms phase difference is a rapidly increasing function of the separation distance if the separation is less than the internal wave length scale, 2 to 3 km for a horizontal array or 350 m for a vertical array*. The rms phase difference increases more slowly for greater separation distances. At 150 Hz and 50 km range, the rms phase difference is expected to be quite small for both the Arctic and the Gulf of Alaska, but it is expected to be much larger in the Newfoundland Basin, mainly because

* Using Desaubies scaling, these numbers become 3 to 4 km for a horizontal array and 300 to 700 m for a vertical array.

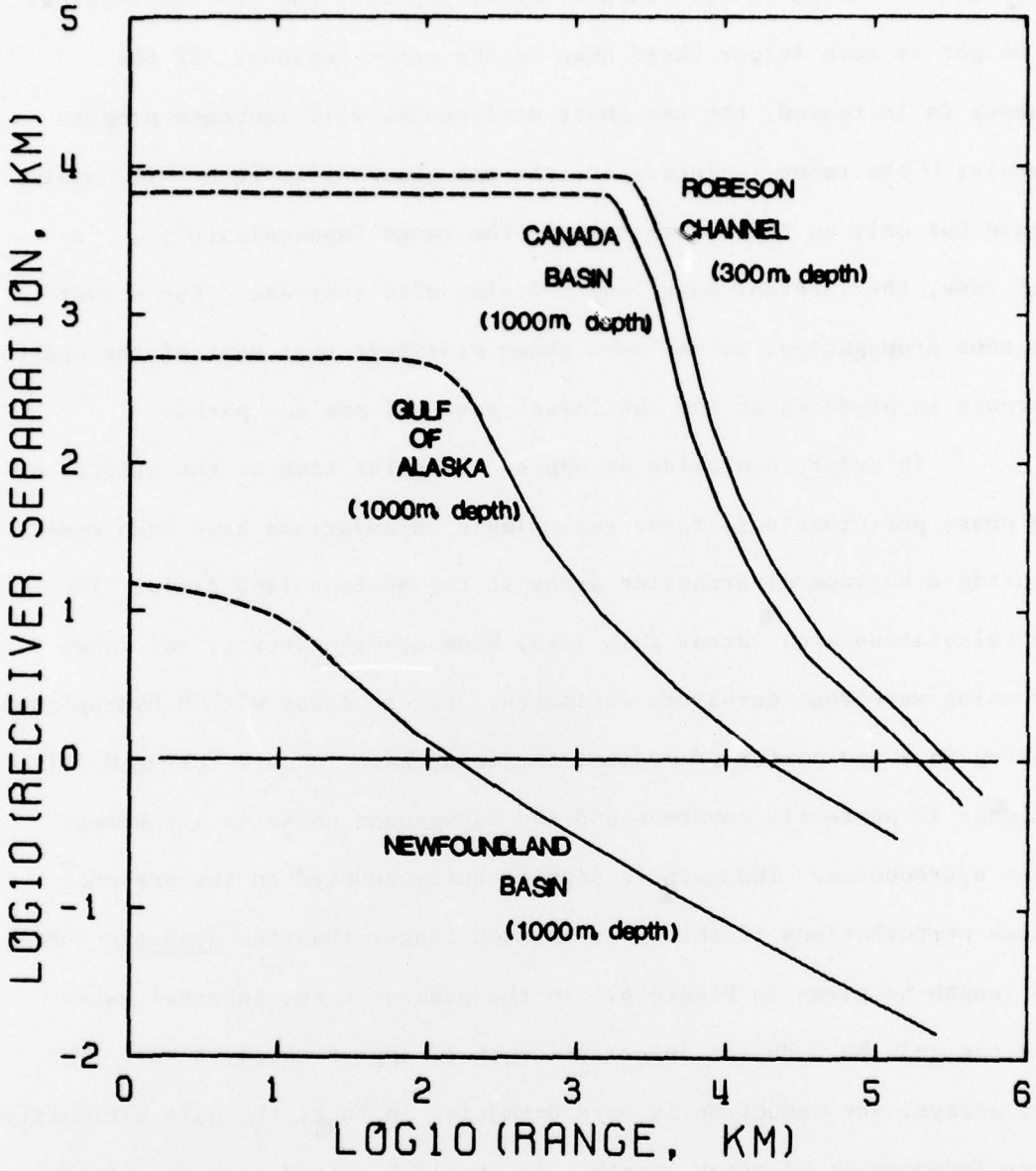

Figure 6. Horizontal broadside receiver separation vs. range for acoustic coherence of 0.5 at 150 Hz.

the product of the potential sound velocity gradient and the rms internal wave height is much larger there than in the other regions. If the frequency is increased, the rms phase differences will increase proportionately; if the range is increased, the rms phase differences will again increase but only as the square root of the range (approximately). In either case, the internal wave length scales will increase. For convergence zone propagation, it has been shown elsewhere that most of the phase difference is produced at the shallowest parts of the ray paths.

In order to provide an appreciation for some of the effects of these phase perturbations, three very simple calculations have been made, each using a horizontal broadside array in the Newfoundland Basin. The three calculation are: array gain loss, beam steering error, and range error using wavefront curvature estimates. For an array with M hydrophones operating in a non-perturbed medium, the array gain in dB is 10 log(M) if the signal is perfectly coherent and the background noise is incoherent between hydrophones. The gain is significantly reduced in the presence of phase perturbations if the array is much longer than the acoustic coherence length as given in Figure 6. In the present case, internal waves reduce the gain by 3 dB for an array length of approximately 5 km*. For larger arrays, the reduction is more dramatic, in fact, the gain ultimately becomes independent of array length. It should be noted that this loss is frequency and range dependent; the loss will increase as the range increases and decrease as the acoustic frequency decreases. It should also be noted that 'approximately 5 km' is only coincidentally the same as the

---

* For a horizontal endfire array the necessary array length for 3 dB loss is approximately 12 km; for a vertical broadside array, it is approximately 250 m.

the internal wave coherence length, 4.7 km. The beam steering error is very small. Even if only two hydrophones are used, the rms steering error is less than 0.1^{o} for a hydrophone separation greater than 700 m, and the error decreases as the separation increases. It is expected that less error would result if a statistical estimation method were employed using more than two hydrophones. This error is frequency independent and it increases approximately as the square root of the range. The range estimation error using wavefront curvature is also frequency independent and decreases as the hydrophone separation increases; however, it increases as approximately the 3/2's power of the range. At least three hydrophones are necessary to form the estimate, and, for the present case, with equal hydrophone spacings of 0.5 km, the rms range error using only 3 hydrophones is 15% of the range. If more than three hydrophones are used with a statistical fitting technique, this error will probably decrease.

The model that has been presented here is highly simplified and rather loosely applied, partly because it assumes that the Garrett-Munk (or Desaubies) internal wave spectrum applies equally well everywhere. There is evidence that it applies in the temperate oceans (Desaubies, 1976a); as yet no evidence has been published concerning its applicability in the Arctic. The other important simplification is that the potential sound velocity gradient and the rms internal wave height are depth-independent. More specifically, the assumption is that the product $(\partial c_p/c_o \partial z)^2 \lambda_H^2 \zeta_{rms}^2$ is constant along an acoustic ray, and, for medium to long ranges, this is equivalent to the previous statement. The variation of this product is largely controlled by the term $(\partial c_p/\partial z)^2/n(z)$ and this in turn is controlled by the local potential temperature gradient and the local salinity gradient.

Munk (1974, his equation (10)) shows that $\partial c_p/\partial z$ and $n^2(z)$ are proportional; he also shows that the "constant" of proportionality is a function of the Turner number, that is, a number which is proportional to the ratio of the local salinity and potential temperature gradients. The term $(\partial c_p/\partial z)^2/n(z)$ can therefore be expected to vary with depth and with geographical location. As shown earlier for the Garrett-Munk profile, it varies approximately with depth as $e^{-3z/b}$, and from this it can be seen that it reduces by a factor of 20 if the ray depth increases by an amount equal to b. This reduction factor will be at least partly offset by the fact that the rays must necessarily be non-horizontal over part of the path, probably that part nearest the surface, and thus for the "horizontal configuration" cases, scattering will be partly due to the vertical structure of the internal wave field at depths when the vertical structure is strongest. This structure possesses shorter coherence lengths and can produce much larger phase differences than the horizontal structure (c.f. Table II and note that the vertical receiver separation is only 50 m whereas the horizontal receiver separation is 1000 m). The overall effect, then, of this simplification is in fact unknown, but it is expected that it will result in estimates of ϕ^2 that are too large.

Removal of other simplifications in the work presented here (e.g. only three array configurations) or extensions to other geographical regions could be done straightforwardly.

REFERENCES

Briscoe, M.G., (1975), "Oceanic Internal Waves", reprinted from J. Geophys. Res., 80, American Geophysical Union.

Chen, C-T and F.J. Millero, (1976), "The Specific Volume of Seawater at High Pressures", Deep-Sea Res., 23, 595-612.

Desaubies, Y.J.F., (1976a), "Analytical Representation of Internal-Wave Spectra", J. Phys. Oceanog., 6, 6, 976-981.

Desaubies, Y.J.F., (1976b), "Acoustic-Phase Fluctuations Induced by Internal Waves in the Ocean", J. Acoust. Soc. Am., 60, 4, 795-800.

Fofonoff, N., (1962), "The Sea", Vol. 1, p. 15, M.N. Hill (General Editor), Interscience Publishers.

Hashimoto, E., (1968), "Average Winter and Summer Temperature and Salinity Profiles for the Deep Ocean Provinces", Technical Note #41, Fleet Numerical Weather Central, Monterey, CA., U.S.A.

Helinveaux, R.H., (1963), "Oceanographic Observations in the Canadian Basin Arctic Ocean, April-May 1962", Manuscript Report Series (Oceanographic and Limnological) #144, Pacific Oceanographic Group, Nanaimo, B.C., Fisheries Research Board of Canada.

Munk, W.H., (1974), "Sound Channel in an Exponentially Stratified Ocean, with Applications to SOFAR", J. Acoust. Soc. Am., 55, 2, 220-226.

Munk, W.H. and F. Zachariasen, (1976), "Sound Propagation through a Fluctuating Stratified Ocean: Theory and Observations", J. Acoust. Soc. Am., 59, 4, 818-838.

Sadler, H.E., (1976), "The Flow of Water and Heat through Nares Strait", DREO Report #736, Defence Research Establishment Ottawa, National Defence Headquarters, Ottawa, Ont., K1A 0Z4, Canada.

APPENDIX A

DESAUBIES' SCALING FOR THE GARRETT-MUNK SPECTRUM

Using Desaubies' scaling, Eq. (8b) becomes

$$\phi^2 = \left(\frac{\omega}{c_o}\right)^2 \left(\frac{\partial c_p}{c_o \partial z}\right)^2 \frac{2r}{\pi n} \{\lambda(90^o)\}^2 \{\tan^{-1}\sqrt{\mu^2 - 1} - \sqrt{\mu^2 - 1}/\mu^2\} T, \quad \text{(A1)}$$

or, with $\mu = \infty$ and $r = 300$ m^{2}cph,

$$\text{rms } \phi = 6235 \left(\frac{\partial c_p}{c_o \partial z}\right) \frac{\lambda_H}{\lambda_a} \sqrt{\frac{T_\infty}{n}} \text{ degrees} \quad \text{(A2)}$$

where $T_\infty = T$ at $\mu = \infty$, n is expressed in cph, and SI units are used elsewhere. Also, from (9a) and (9b)

$$\lambda_H = \frac{1}{8tn_{in}} \frac{\tan^{-1}\sqrt{\mu^2 - 1} - \sqrt{\mu^2 - 1}/\mu^2}{\ln \mu - (\mu^2 - 1)/2\mu^2}, \quad \text{(A3)}$$

$$\lambda_v = \frac{1}{2\pi t n_{in}} \frac{1}{\mu}.$$

With $\mu >> 1$ and $t = 3\ 10^{-4}$ (cycles per metre)/cph,

$$\lambda_H = 654.5/(n_{in} \ln \mu),$$

$$\lambda_v = 530.5/n.$$

Table A1 shows the results equivalent to Table II but calculated using the local measured value of n(z) and using (A1, A3 and A4). The main difference from the Table II values occurs for the Arctic case; Desaubies'

scaling predicts more phase fluctuation and longer internal wave length scales than the Garrett-Munk scaling. In fact, according to Table A1, the Arctic and Gulf of Alaska display essentially the same degree of instability. The Newfoundland Basin is again predicted to be the most unstable but this time with the shortest vertical internal wave length scale instead of the longest.

TABLE A1

DESAUBIES' MODEL - Phase difference for a range of 50 Km, an acoustic frequency of 150 Hz and a receiver separation of either 1 km (horizontal case) or 50 m (vertical case).

Region and Depth	n(cph)	Horizontal Broadside rms $\phi = \langle[\phi(R_2)-\phi(R_1)]^2\rangle^{\frac{1}{2}}$			λ_H	λ_V
		Endfire Horizontal	Broadside Horizontal	Broadside Vertical		
Gulf of Alaska (1000 m)	1.20	1.3^o	3.9^o	3.5^o	4.0 km	450 m
Newfoundland Basin (1000 m)	2.55	11^o	31^o	39^o	3.6 km	280 m
Robeson Channel (April, 300 m)	1.97	1.1^o	3.4^o	2.0^o	3.7 km	590 m
Canada Basin (April, 1000 m)	.66	$.74^o$	2.2^o	1.1^o	4.0 km	720 m

APPENDIX B

MATHEMATICAL DETAILS LEADING TO THE FINAL EXPRESSION FOR ϕ^2.

In Eq. (7) on page 6 the term $\langle\zeta(\vec{x}_1)\zeta(\vec{x}_2)\rangle$ is the correlation function, R_ζ, of the internal wave spectrum. This in turn is the Fourier transform of the power spectrum in wave number space, and it can be shown that the slant range correlation is given by

$$R_\zeta(H,V) = \int_{n_{in}}^{n(z)} d\omega \int_0^\infty d\alpha\ \overline{Z^2}\ E(\alpha,\omega)\ \cos\left[2\pi\alpha V\left(\frac{n^2-\omega^2}{\omega^2-n_{in}^2}\right)^{\frac{1}{2}}\right] J_o(2\pi\alpha H) \qquad (B1)$$

where $\overline{Z^2} = b^2 n_o \dfrac{\omega^2-n_{in}^2}{n\omega^2}$, $E(\alpha,\omega) = \dfrac{2}{\pi}\, EA(\lambda)\, \dfrac{n_{in}}{\omega(\omega^2-n_{in}^2)^{\frac{1}{2}}\alpha_*}$, $A(\lambda) = (2/\pi)(1+\lambda^2)^{-1}$, $\lambda = \alpha/\alpha_*$, $\alpha_* = (3/2n_o b)\sqrt{\omega^2-n_{in}^2}$, H = horizontal component of $\overrightarrow{x_1-x_2}$, V is the vertical component of $\overrightarrow{x_1-x_2}$, and α is expressed in cycles per metre (see Desaubies 1976a, Eq. 10, and note that $R_\zeta(H,V)$ as given in (B1) is the same as his $\int_0^\infty d\omega\ MSC(\omega)\ MS(\omega)$). By substituting this expression in (7) and taking the gradient $\dfrac{\partial c_p}{c_o \partial z}$ outside the integral signs (because they are assumed constant over the propagation path), the mean-square phase difference becomes

$$\phi^2 = \frac{\omega^2}{c_o^2}\left(\frac{\partial c_p}{c_o \partial z}\right)^2 \frac{2}{\pi} Eb^2 \left(\frac{n_o}{n}\right) \frac{2}{\pi}\int_1^\mu dx\ \frac{\sqrt{x^2-1}}{x^3}\int_0^\infty du \left\{\iint_0^{R_1R_2} + \iint_0^{R_1R_2} - 2\iint_0^{R_1R_2}\right\} dr_1 dr_2 \frac{\cos\left(\frac{3\pi n_{in}}{n_o b} V\sqrt{\mu^2-x^2}\ u\right) J_o\left(\frac{3\pi n_{in}}{n_o b} H\sqrt{x^2-1}\ u\right)}{1+u^2} \qquad (B2)$$

In this expression, V and H are function of r_1 and r_2, but their functional forms are not necessarily the same for each of the three double integrals in r_1, r_2. For the horizontal endfire configuration, they <u>are</u> all the same: $V = 0$, $H = |r_1 - r_2|$, with $R_1 = R - \Delta/2$ and $R_2 = R + \Delta/2$; however, for the horizontal broadside configuration, $V = 0$, $H = r_1 - r_2$ for the first two integrals and $H = \sqrt{\{(r_1 - r_2)^2 + (r_1 + r_2)^2\, \Delta^2/4R^2\}/\{1 + \Delta^2/4R^2\}}$, with $R_1 = R_2 = \sqrt{R^2 + \Delta^2/4}$, where Δ is the hydrophone separation distance. For the vertical broadside case, again the first two are the same, $V = \frac{1}{2}\,|r_2 + r_1|\,\Delta/\sqrt{R^2 + \Delta^2/4}$, $H = |r_2 - r_1|R/\sqrt{R^2 + \Delta^2/4}$, and the third is $V = (\Delta/R)\,(r_2 \pm \frac{1}{2}\sqrt{(r_2 - r_1)^2 + 2(r_1^2 - r_2^2)\,\Delta^2/4R^2 + (r_2 + r_1)^2\,\Delta^4/16R^4})$ $X(1 + \Delta^2/4R^2)^{-3/2}$, $H = (r_2\Delta^2/2R^2 \pm \sqrt{(r_2 - r_1)^2 + 2(r_1^2 - r_2^2)\Delta^2/4R^2 + (r_2 + r_1)^2\Delta^4/16R^4})$ $X(1 + \Delta^2/4R^2)^{-3/2}$, with $R_1 = R_2 = \sqrt{R^2 + \Delta^2/4}$. The general form given in (B2) can be further simplified by replacing $J_o(z)$ with $2/\pi \int_o^{\pi/2} \cos(z\sin\theta)\,d\theta$. The two cosine terms have arguments that are linear in u and they can be combined. The integration in u can be carried out with the help of the formula $\int_o^\infty du\, \cos(ua)/(1 + u^2) = \pi/2\; e^{-|a|}$:

$$\phi^2 = \frac{\omega^2}{c_o^2}\left(\frac{\partial c_p}{c_o \partial z}\right)^2 \frac{2}{\pi}\, Eb^2\left(\frac{n_o}{n}\right) \frac{2}{\pi}\int_1^\mu dx\, \frac{\sqrt{x^2 - 1}}{x^3}\left[\left\{\iint_o^{R_1} + \iint_o^{R_2} - 2\iint_o^{R_1 R_2}\right\} dr_1 dr_2\right.$$

$$\left. \times \frac{1}{2}\int_o^{\pi/2} d\theta \left\{ e^{\frac{-3\pi n_{in}}{n_o b}\left|V\sqrt{\mu^2 - x^2} + H\sqrt{x^2 - 1}\,\sin\theta\right|} \right.\right. \qquad \text{(B3)}$$

$$\left.\left. + e^{\frac{-3\pi n_{in}}{n_o b}\left|V\sqrt{\mu^2 - x^2} - H\sqrt{x^2 - 1}\,\sin\theta\right|} \right\}\right]$$

In all cases, the integrals in r_1 and r_2 can be carried out, but, because of algebraic complexities, only the horizontal endfire case will be shown here. For this case, $V = 0$ and $dr_1\, dr_2$ can be converted to $dr\, dH$ with

appropriate sets of limits. The integrals can then be done by parts and the final result is

$$\phi^2 = \frac{\omega^2}{c_o^2}\left(\frac{\partial c_p}{c_o \partial z}\right)^2 \frac{2}{\pi} Eb^2\left(\frac{n_o}{n}\right) \frac{2}{\pi}\int_o^{\pi/2} d\theta \int_1^{\mu} dx \left(\frac{n_o b}{3\pi n_{in}}\right)^2 \frac{2}{x^3(x^2-1)^{\frac{1}{2}}\sin^2\theta}$$

$$\times\left\{e^{\frac{-3\pi n_{in}}{n_o b}\Delta\sqrt{x^2-1}\sin\theta} + \frac{3\pi n_{in}}{n_o b}\Delta\sqrt{x^2-1}\sin\theta - 1\right\}. \qquad \text{(B4)}$$

The combination of parameters $n_o b/3\pi n_{in}$ is proportional to λ_H (see Eq. 9a), and, in the limit $\Delta \to o$, the double integral becomes $\frac{2}{\pi}\Delta^2\{\tan^{-1}\sqrt{\mu^2-1} - \sqrt{\mu^2-1}/\mu^2\}$. Introducing these terms explicitly into (B4) produces

$$\phi^2 = \frac{\omega^2}{c_o^2}\left(\frac{\partial c_p}{c_o \partial z}\right)^2 \frac{2}{\pi} Eb^2\left(\frac{n_o}{n}\right) \lambda_H^2 \{\tan^{-1}\sqrt{\mu^2-1} - \sqrt{\mu^2-1}/\mu^2\}T, \qquad \text{(B5)}$$

$$T = \frac{\frac{2}{\pi}\int_o^{\pi/2} d\theta \int_1^{\mu} dx \frac{2}{P^2(\mu)x^3(x^2-1)^{\frac{1}{2}}\sin^2\theta}\left\{e^{\frac{-\Delta}{\lambda_H}P(\mu)\sqrt{x^2-1}\sin\theta} + \frac{\Delta}{\lambda_H}P(\mu)\sqrt{x^2-1}\sin\theta - 1\right\}}{\tan^{-1}\sqrt{\mu^2-1} - \sqrt{\mu^2-1}/\mu^2} \qquad \text{(B6)}$$

$$P(\mu) = \frac{\pi}{4}(\tan^{-1}\sqrt{\mu^2-1} - \sqrt{\mu^2-1}/\mu^2)/(\ln\mu - (\mu^2-1)/2\mu^2) \qquad \text{(B7)}$$

The transformation just introduced, and the resulting equation (B5), are also valid for the general case. For the endfire configuration, it can be seen that T is independent of range, and, as $\Delta \to o$, $T \to \frac{1}{2}(\Delta/\lambda_H)^2$, independent of μ. (As $\Delta \to \infty$, $T \to (\frac{32}{\pi^4} \ln\mu)\frac{\Delta}{\lambda_H}\ln\frac{\Delta}{\lambda_H}$.)

In general, the rms internal wave height ζ_{rms} can be obtained from (B1) at H = V = 0:

$$\zeta_{rms} = \sqrt{R_\zeta(0,0)} = \left\{ \int_{n_{in}}^{n(z)} d\omega \int_0^\infty d\alpha \; \overline{Z^2} \; E(\alpha,\omega) \right\}^{\frac{1}{2}}$$

$$= \left[\tfrac{1}{2} E b^2 \; \frac{n_o}{n} \; \frac{2}{\pi} \left\{ \tan^{-1} \sqrt{\mu^2 - 1} \; - \sqrt{\mu^2 - 1}/\mu^2 \right\} \right]^{\frac{1}{2}}$$

Also, $\omega/c_o = 2\pi/\lambda_{acoustic}$. Eq. (B5) can be rewritten using these definitions, and the result is (8a). The general form of T can be obtained by comparing (B5) and (B3):

$$T = \left\{ \frac{2}{\pi} \int_1^\mu dx \frac{\sqrt{x^2-1}}{x^3} \left[\left\{ \iint_0^{R_1 R_2} + \iint_0^{R_1 R_2} - 2 \iint_0^{R_1 R_2} \right\} \frac{dr_1 dr_2}{\lambda_H^2} \int_0^{\pi/2} d\theta \left\{ e^{-\left| \frac{V}{\lambda_V} \sqrt{1-x^2}/\mu^2 + \frac{H}{\lambda_H} P(\mu) \sqrt{x^2-1} \sin\theta \right|} \right.\right.\right. \tag{B8}$$

$$\left.\left.\left. + e^{-\left| \frac{V}{\lambda_V} \sqrt{1-\frac{x^2}{\mu^2}} - \frac{H}{\lambda_H} P(\mu) \sqrt{x^2-1} \sin\theta \right|} \right\} \right] \Big/ \left\{ \tan^{-1} \sqrt{\mu^2 - 1} \; - \sqrt{\mu^2 - 1}/\mu^2 \right\}$$

The functional description of T in (8b) is equivalent to (B8).